

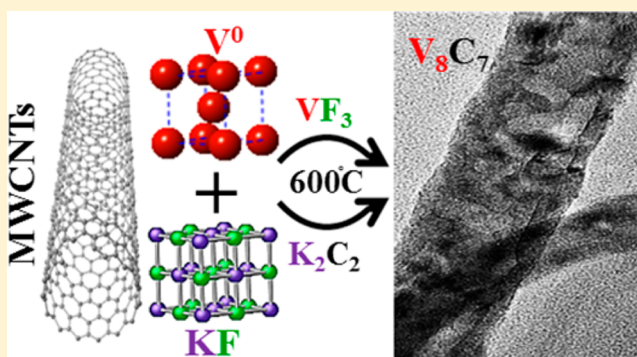
Formation Mechanism of Nanostructured Metal Carbides via Salt-Flux Synthesis

Samantha M. Schmuecker and Brian M. Leonard*

Department of Chemistry, University of Wyoming, Laramie, Wyoming 82071, United States

Supporting Information

ABSTRACT: Nanostructured metal carbides are of particular interest because of their potential as high surface area, low-cost catalysts. By taking advantage of a salt-flux synthesis method, multiple carbide compounds were synthesized at low temperatures providing a pathway to nanosized materials. To better understand the reaction mechanism, vanadium carbide (V_8C_7) synthesis was monitored by quenching samples at 100 °C intervals and analyzed by multiple spectroscopic methods. The reaction was determined to occur through the formation of metal halide and acetylide carbide intermediates, which were repeatedly observed by X-ray diffraction and further supported by IR and Raman spectroscopies. Control experiments were also employed to further verify this mechanism of formation by using different salt compositions and a solid-state metathesis reaction. The reaction mechanism was also verified by applying these techniques to other metal carbide systems, which produced similar intermediate compounds.



INTRODUCTION

Metal carbides are experiencing a resurgence in popularity due to their interesting physical properties, low cost, and potential catalytic activity.¹ Metal carbides are some of the hardest materials known with hardness values approaching that of diamond.² These compounds are also quite stable, resistant to oxidation and acid etching, electrically conducting, and superconducting.³ They are also some of the highest melting compounds ever synthesized with melting points greater than 3000 °C.⁴ While this is useful for several high-temperature applications, it also causes problems with synthesizing these materials. Some of the more common methods used to synthesize metal carbides including arc melting, high-temperature annealing, and carbothermic reduction require extremely high temperatures, which causes aggregation and greatly decreases the surface area of the product.^{5–7} As such, very few metal carbide systems have been reported as nanomaterials.⁸

One of the major problems with traditional solid-state synthesis is slow diffusion between solids. While some methods have been developed to overcome this limitation like modulated elemental reactants, many methods still use extremely high temperatures to increase the rate of diffusion.⁹ A few low-temperature synthesis methods have been reported for metal carbide synthesis, like sonochemical and alkalide reduction; however most of these methods focus on molybdenum carbide and tungsten carbide.^{8,10} Additionally, these synthesis methods commonly use metal oxide precursors and produce materials with residual oxygen present in the lattice.¹¹

Salt fluxes have been used to synthesize a variety of materials including oxides, pnictides, chalcogenides, halides, and carbides.^{12–15} This synthesis technique offers enhanced reaction rates due to a molten or liquid reaction medium.¹⁶ The flux enables faster diffusion of the reactants and thus enables lower reaction temperatures and shorter annealing times. Utilizing eutectic mixtures of binary salts, the melting point of the flux can be dramatically reduced giving access to high-temperature products at unusually low temperatures. While this is a frequently used method, little is known about how these reactions occur.¹³ Further, determining the optimal reaction time and temperatures to this point has been primarily trial and error. Solid-state reaction mechanisms are inherently quite difficult to study due to the high reaction temperatures and the inability to directly monitor the reaction as it progresses. While some methods like thermogravimetric analysis (TGA) and differential scanning calorimetry (DSC) have been developed to peek inside of this black box, these techniques only provide a partial view of the reaction and cannot identify crucial intermediates or reaction processes.

To study these reactions and the intermediate species that form, the three carbide systems of vanadium carbide (V_8C_7), titanium carbide (TiC), and tantalum carbide (TaC) were analyzed. For each system, the reactions were quenched at multiple temperature intervals and evaluated with a variety of spectroscopic methods. This quick cooling freezes or solidifies the salt flux stopping the reaction immediately and trapping

Received: January 14, 2015

Published: March 30, 2015

intermediate compounds. Since the salt fluxes are transparent to IR and Raman spectroscopy, the flux allows a detailed study of the sample including air- and moisture-sensitive compounds. In addition, X-ray diffraction (XRD) allows observation of the bulk sample including all crystalline materials present. With the wide range of salts available for fluxes, salts can be chosen to limit overlapping diffraction peaks allowing for positive identification of all species present. Finally, different cations and anions can be evaluated for their involvement in the reaction through control reactions.

Utilizing this method, several important intermediates were observed forming, decomposing, and finally giving rise to the formation of the target metal carbides. The mechanism discussed herein is the best estimate of how this synthetic method produces metal carbide compounds, through metal halide (MF_3) and acetylide carbide (K_2C_2) intermediates. Applying this method to study the reaction mechanism will help determine product formation temperatures and optimize reaction conditions. This will greatly reduce guesswork involved in synthesis by determining exact temperatures at which intermediate species are formed and subsequently decompose to form the product.

EXPERIMENTAL SECTION

Materials. All the chemicals were purchased from Sigma-Aldrich. All salts were dried in a drying oven at 100 °C for 1 h prior to use and stored in a desiccator. The metal reagents were stored in an argon-filled glovebox due to their oxidative and pyrophoric properties.

Synthesis. For the preparation of the vanadium carbide, vanadium metal powder (−325 mesh) (0.2023 g = 0.004 mol) and multiwalled carbon nanotubes (MWCNTs) (6–9 nm × 5 μm with a carbon >95% purity) (0.0477 g = 0.004 mol) were weighed and added to a salt mixture consisting of 58 wt % lithium chloride (0.2243 g), 40 wt % potassium chloride (0.2764 g), and 2 wt % of potassium fluoride (0.0100 g). The reactants were ground with a mortar and pestle for 5 min to ensure homogeneity. All weighing and grinding should be done in an oxygen free environment to prevent oxidation of the vanadium metal and hydration of the salt flux. However, sample preparation for this work was not done in an oxygen-free environment due to the relatively low humidity of the lab, proving that, while air-sensitive, these reactions can be done outside of a glovebox. After grinding, the reactants were placed in an alumina crucible and heated at 100 °C/hour in a tube furnace to the desired temperatures under flowing argon. Most samples were quickly cooled (quenched) upon reaching the given interval temperature, to stop the reaction and trap the intermediates. The samples were quenched by removing the reaction tube from the heating coils and allowing them to quickly cool ~800 °C per hour to room temperature (25 °C) during which the freezing temperature of the eutectic salt is obtained quickly, below 353 °C. However, a few samples were annealed at the final temperature for 2 h as will be discussed in the Results section. Similar methods were used for the synthesis of TiC and TaC using a 1:1 molar ratio for metal and carbon.

Characterization. Powder XRD patterns were obtained with a Rigaku Smart Lab (40 kW) X-ray diffractometer using Cu K α radiation ($\lambda = 1.54059 \text{ \AA}$). Raman and infrared spectra were acquired with Snowy Range Instruments Raman Sierra IM-52 using a 532 nm laser and a PerkinElmer FTIR Spectrometer Spectrum Two with a Pike Technologies GladiATR attachment, respectively. TGA and DSC were conducted on a TA Instruments SDT Q600 under argon with a flow rate of 100 mL/min. Transmission electron microscopic (TEM) images were taken on a 200 kV FEI Tecnai G2 F20 (S)TEM with an Oxford Inca X-Stream EDX Spectrometer. TEM samples were prepared by adding ~0.3 mg of sample into a vial with ~10 mL of ethanol. The solution was then sonicated for 20 min until slightly gray, and a micropipette was used to drop ~7 μL of the suspension onto a 300 mesh holey nickel grid and dried overnight.

RESULTS AND DISCUSSION

To investigate the formation of metal carbides utilizing a salt flux, a mixture of MWCNTs, metal powder, and the salt flux (LiCl, KCl, and KF) were ground together and heated in a tube furnace to several temperatures at 100 °C intervals and quenched to trap intermediate species. The products present were analyzed without further purification to prevent loss of any water-soluble intermediates. To achieve clean metal carbide nanomaterials, the samples are typically washed with distilled water to remove any remaining salts from the products. Each sample was analyzed with powder XRD, TEM, Raman, and IR spectroscopies. The results shown below provide evidence of intermediate species and give insight into the reaction mechanism.

The overall XRD spectra for all temperature intervals can be seen in Figure 1a, and all phases observed by XRD are reported

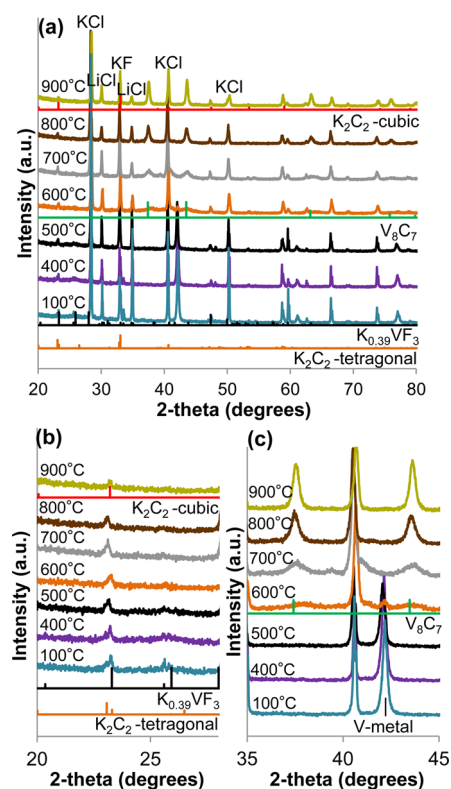


Figure 1. XRD plots of (a) the reaction between vanadium metal and MWCNTs in salt flux at multiple temperatures. (b) Highlighted: the formation and decomposition of $\text{K}_{0.39}\text{VF}_3$ (PDF# 00–033–1051),¹⁷ K_2C_2 -tetragonal (PDF# 01–076–1714),¹⁸ and K_2C_2 -cubic (PDF# 01–070–3190).¹⁹ (c) The decomposition of V metal (PDF# 01–089–3842)²⁰ and the formation of V_8C_7 (PDF# 03–065–8074).²¹

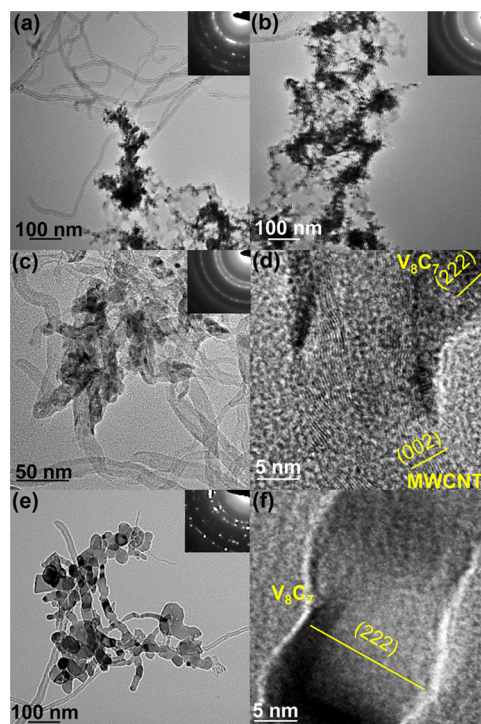
in Table 1. Analysis of these data shows the formation of potassium vanadium trifluoride ($\text{K}_{0.39}\text{VF}_3$) at 100 °C indicated by reflections (002), (430), (440), (260), and (232).¹⁷ See Supporting Information, Table S1 for peak positions and associated reflections for all phases present. Tetragonal potassium acetylide (K_2C_2) is also formed at 100 °C, represented by reflections (200), (004), and (202).¹⁸ K_2C_2 then undergoes a phase change to cubic K_2C_2 that is formed at 200 °C (omitted for clarity), and is observed between 400 and 1000 °C by reflections (111), (200), and (220).¹⁹ The $\text{K}_{0.39}\text{VF}_3$ intermediate is stable up to 500 °C, which is most clearly seen in Figure 1b. It is quite difficult to determine the amount of V

Table 1. Phases Observed by XRD for All Temperature Intervals

temperature,	V_8C_7 results
100 °C	KCl+LiCl+KF+V ⁰ +K _{0.39} VF ₃ +K ₂ C ₂ -tetragonal
200 °C	KCl+LiCl+KF+V ⁰ + K _{0.39} VF ₃ +K ₂ C ₂ -cubic
300 °C	KCl+LiCl+KF+V ⁰ +K _{0.39} VF ₃ +K ₂ C ₂ -cubic
400 °C	KCl+LiCl+KF+V ⁰ +K _{0.39} VF ₃ +K ₂ C ₂ -cubic
500 °C	KCl+LiCl+KF+V ⁰ +K _{0.39} VF ₃ +K ₂ C ₂ -cubic
600 °C	KCl+LiCl+KF+V ⁰ +K ₂ C ₂ -cubic +V ₈ C ₇
700 °C	KCl+LiCl+KF+K ₂ C ₂ -cubic +V ₈ C ₇
800 °C	KCl+LiCl+KF+K ₂ C ₂ -cubic +V ₈ C ₇
900 °C	KCl+LiCl+KF+K ₂ C ₂ -cubic +V ₈ C ₇
1000 °C	KCl+LiCl+KF+K ₂ C ₂ -cubic +V ₈ C ₇

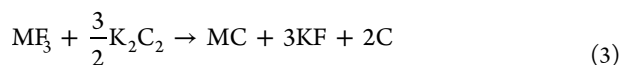
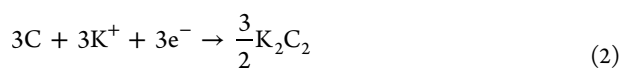
metal and K_{0.39}VF₃ due to overlapping reflections with the salt flux; however, it is clear that some K_{0.39}VF₃ forms at low temperatures and decomposes near the decomposition temperature of the V metal. At 600 °C, the K_{0.39}VF₃ decomposes, and the vanadium metal reflection (110) decreases significantly as can be seen in Figure 1b,c.²⁰ Concurrently, vanadium carbide (V₈C₇) begins to form as small, very broad reflections of (111) and (200).²¹ While it is assumed that the V metal should all be converted to K_{0.39}VF₃ prior to formation of V₈C₇, the K_{0.39}VF₃ phase appears to be unstable at these temperatures and quickly decomposes to form V₈C₇. This suggests the formation of K_{0.39}VF₃ is a limiting step and the decomposition process at elevated temperatures is relatively quick. Above 600 °C the V₈C₇ continues to form and the K₂C₂ remains stable up to 1000 °C shown in Figure 1b,c. Probing intermediate temperatures confirm that the K_{0.39}VF₃ decomposes by 550 °C and the V₈C₇ has begun to form as seen in Supporting Information, Figure S1. Additionally, Supporting Information, Figure S2 shows the products of a reaction at 500 °C, which was held for 12 h, demonstrating the complete decomposition of V metal and the formation of V₈C₇ at 500 °C.

In addition to XRD, TEM was used to examine the products of these reactions. Because of the use of ethanol in the preparation of the TEM grids and the intermediates' solubility in water and ethanol, none of the intermediates (K₂C₂ or K_{0.39}VF₃) were observed via TEM. In Figure 2, TEM images were taken of samples heated to 500, 600, and 900 °C displaying the transformation of V metal and MWCNTs to V₈C₇. These temperatures were chosen based on the XRD plots, which showed the transition from reactants to V₈C₇ occurring at 600 °C. At 500 °C, most of the sample consists of vanadium metal and MWCNTs as seen in Figure 2a and the inset selected area electron diffraction (SAED). The metal has decreased in size from the starting material (~20 μm) to 10–50 nm aggregates. Supporting Information, Figure S3 shows the as-purchased V metal with particles sizes ranging from 2 to 20 μm. This suggests that the metal is reacting, which supports the XRD results showing a decrease in V metal intensity and formation of K_{0.39}VF₃ below 500 °C. However, in Figure 2b, the same 500 °C sample reveals V₈C₇ in a small amount, demonstrated by SAED ring patterns specific to the crystal planes associated with V₈C₇. This was not observed at 500 °C by XRD because it is a bulk analysis technique and V₈C₇ is below the detection limits. SAED, however, has a higher sensitivity to phase identification because it is a particle to particle analysis technique. Figure 2c,d shows images of the sample heated to 600 °C showing V₈C₇ with a hollow tubelike structure where the lighter contrast tubes are MWCNTs, and

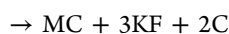
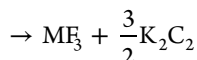
**Figure 2.** TEM images and SAED of the reaction between V metal and MWCNTs at (a, b) 500 °C (c, d) 600 °C and (e, f) 900 °C.

the darker tubes are V₈C₇. Figure 2d highlights the formation of V₈C₇ around a MWCNT providing further evidence that the MWCNT acts as a template for the carbide. The lattice fringes depicted in Figure 2d represent the (002) crystal plane ($d = 3.348$ Å) of the MWCNTs and the (222) crystal plane ($d = 2.405$ Å) of V₈C₇. Additionally, multiple lattice fringes can be observed in the V₈C₇, thus proving that it is polycrystalline. Supporting Information, Figure S5 shows a larger version of this image with multiple lattice fringes for both the MWCNT and V₈C₇. SAED also confirms the formation of V₈C₇ nanocrystals in the 600 °C sample, which is in agreement with XRD. Figure 2e,f shows results of the sample heated to 900 °C and shows larger crystal domains of V₈C₇ strung together into nanowires. Between 600 and 900 °C, the hollow tube structure coalesced into a solid wire of roughly similar size (~25 nm) as seen in Figure 2c,e. The formation of V₈C₇ was observed through our experiments to begin at ~600 °C based on XRD, and confirmed by SAED. The interesting part was that even though by XRD no V₈C₇ can be seen below 600 °C without annealing, it was observed at 500 °C by SAED in Figure 2b. To confirm this results, V₈C₇ was formed by dwelling at 500 °C for 12 h seen in Supporting Information, Figure S2, which was observed as very broad peaks by XRD confirming the TEM results that the carbide formation does occur at 500 °C.

Reaction Mechanism. On the basis of the XRD data, the proposed mechanism begins with the oxidation of V metal to an approximate V³⁺ state forming K_{0.39}VF₃ (MF₃) intermediate (eq 1). This is assumed to occur simultaneously with the reduction of carbon from the MWCNT to C₂²⁻ to form the K₂C₂ intermediate, shown in eq 2. These two intermediates then react to form V₈C₇ (MC) as seen in eq 3. The overall reaction shows the sum of eqs 1, 2, and 3 from reactants to intermediates to product formation.



overall equation: $M^0 + 3C + 3KF$



$M = V, Ti, \text{ or } Ta$

K_xVF_3 compounds are a well-studied class of materials originating from tungsten-bronze or alkali metal bronze studies. K_xVF_3 compounds have been studied for lattice distortions, superlattice structures, and composition dependent properties.^{22–25} $K_{0.39}VF_3$ forms an orthorhombic structure with lattice constants of $a = 18.34$, $b = 22.19$, and $c = 7.742$ Å, which are in agreement with our experimental results.¹⁷ The melting temperature for K_xVF_3 compounds has been reported to be between 1057 and 1277 °C, proving it is solid and stable at the temperatures used in this study.²⁶

The K_2C_2 intermediate is an acetylide carbide compound that has two phases, a low-temperature tetragonal phase and a high-temperature cubic phase, with the transition occurring at ~ 127 °C.¹⁹ In this study, both phases are observed by XRD with the high-temperature phase forming between 100 and 200 °C, which is in agreement with the reported phase transition. Because one of the main peaks for each of the intermediate species $K_{0.39}VF_3$ and K_2C_2 is closely overlapping at 23.29 and 23.21 degrees 2θ , respectively, further investigation was required to confirm the presence of these species. The reactions of VF_2 and/or VF_3 with KF to form K_xVF_3 compounds have been reported in the literature.²⁷ Since this is a known reaction, the focus of intermediate confirmation will primarily be on K_2C_2 . K_2C_2 has been previously studied by Raman spectroscopy and reported to have a $C\equiv C$ stretching vibration at 1821 cm^{-1} for the acetylide carbon unit (C_2^{2-}).²⁸ To prove the existence of K_2C_2 by Raman, two experiments were designed to increase the total amount of K_2C_2 . The first reaction contained the salt flux, V metal, and MWCNTs, and it was heated to 300 °C for 2 h then quenched. The second sample was identical except no V metal was added to prevent the consumption of K_2C_2 by the reaction with $K_{0.39}VF_3$ forming V_8C_7 . Raman spectra for the samples are shown in Figure 3a. There are relatively small amounts of K_2C_2 in the samples compared to the large amounts of unreacted MWCNTs at 1304 and 1586 cm^{-1} , which are in agreement with literature values. However, a small broad peak is clearly visible at 1820 cm^{-1} for the sample containing V metal and 1825 cm^{-1} for MWCNTs in salt.^{29–31} Similarly, Figure 3b,c shows IR peaks associated with a $C\equiv C$ alkyne (acetylide) stretch at 2156 and 2158 cm^{-1} falling within the range of 2260 – 2100 cm^{-1} (w), further confirming the existence of K_2C_2 in both the vanadium sample and the control reaction.³² The other peaks in the IR spectra are assigned as alkene $C=C$ stretching at 1595 and 1631 cm^{-1} , $C=O$ stretching at 1971 and 2025 cm^{-1} (only in the control), and $O-H$ stretching at ~ 3400 cm^{-1} from absorbed water on both samples.

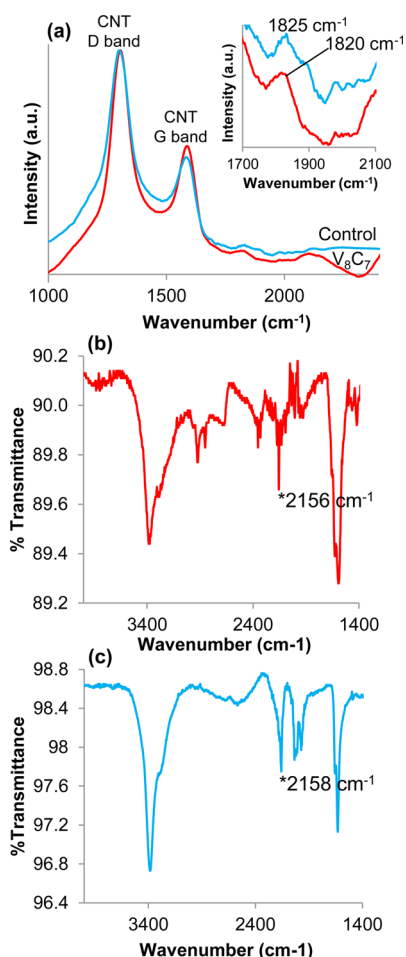


Figure 3. (a) Raman spectra of samples containing V metal and MWCNTs in salt (red) and only MWCNTs in salt (blue) that were heated to 300 °C for 2 h and quenched, showing MWCNT peaks and K_2C_2 peak at 1820 and 1825 cm^{-1} . (b, c) IR spectra of the same samples showing an acetylide carbon peak at 2156 and 2158 cm^{-1} , respectively.

Other Carbide Compounds. To further verify the proposed reaction mechanism, tantalum carbide and titanium carbide were also studied using the same method employed to study V_8C_7 . Figure 4a shows the XRD patterns for titanium carbide, which contains analogous intermediates as vanadium carbide. Titanium trifluoride forms at 100 °C (omitted for clarity) and is stable up to 400 °C. K_2C_2 forms at 100 °C (omitted for clarity) as seen before in the vanadium system and is stable up to 1000 °C. Even though K_2C_2 and TiF_3 peaks are close, (23.07, 23.19 degrees 2θ), they are not as close as those of K_2C_2 and TaF_3 (23.07, 23.11 degrees 2θ), as can be seen in Figure 4a,b, respectively, providing better resolution for the titanium intermediates.^{19,33–35}

Figure 4b shows the XRD results for tantalum carbide demonstrating similar intermediates as vanadium and titanium carbide. It reveals TaF_3 is formed at 100 °C (omitted for clarity) and is stable up to 700 °C indicated by reflections (100), (110), and (111).³⁴ In this system, K_2C_2 does not form until 400 °C and is stable until 1000 °C. However, because of the overlapping of TaF_3 and K_2C_2 's first peak, as well as the second most intense peak for both being hidden by salt peaks, complete certainty cannot be established. The noteworthy aspect is the formation of tantalum carbide starting at 500 °C,

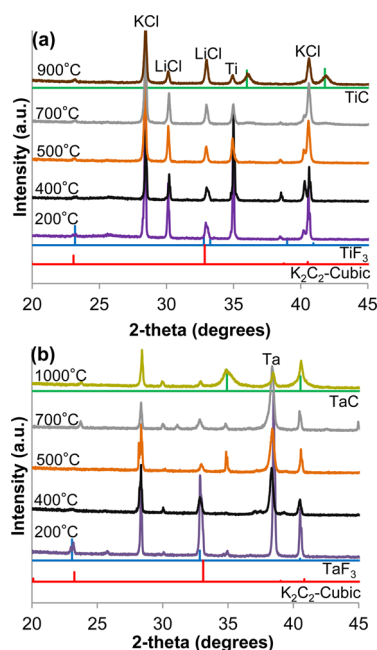


Figure 4. XRD plots (a) TiC temperature intervals, the calculated data is blue for TiF_3 (PDF# 00–009–0112),³³ red for K_2C_2 (PDF# 01–070–3190),¹⁹ green for TiC (PDF# 01–089–3828)³⁵ (b) TaC temperature intervals, the calculated data is blue for TaF_3 (PDF# 01–075–1166),³⁴ red for K_2C_2 , green for TaC (PDF# 00–035–0801).³⁷

the lowest formation temperature through solid state synthesis, which is nearly 300 °C lower than the next lowest formation temperature at ~ 780 °C.^{19,36}

Comparing the three monometallic carbide systems, all three metals oxidized to form a three plus trifluoride compound ($\text{K}_{0.39}\text{VF}_3$, TaF_3 , and TiF_3).³³ Simultaneously, the carbon is reduced by these three electrons and is observed as K_2C_2 intermediate as seen in eq 2. Evidence of the formation of all the trifluorides and K_2C_2 occurs between 100 and 200 °C. The uncertainty of K_2C_2 formation in the TaC system below 400 °C was clarified by the other metal systems and a control reaction, which showed K_2C_2 at 100 °C. The combined reactions of the MF_3 and K_2C_2 intermediates lead to the formation of the transition metal carbide as seen in eq 3. The complete reaction from reactants to final products is seen in the overall equation. The common temperature for the decomposition of the MF_3 intermediate in all three systems was at 500 °C, which correlates strongly with the formation of the transition metal carbide. This provides support for our conclusions that the MF_3 is an important intermediate.

To further support the formation mechanism, control experiments were conducted to establish the necessity of the fluoride ion for intermediate and product formation. Figure 5 shows the reactions of tantalum, carbon, and salt flux without KF present at 600 and 900 °C then quenched. As can be seen from the XRD plots at both temperatures, TaC does not form. Previously, TaC was observed at 900 °C as seen in Supporting Information, Figure S6. However, at 900 °C without KF there is no indication of TaC based on the absence of peaks at 34.93° and $40.55^\circ 2\theta$. There is, however, K_2C_2 formation at both temperatures, which was previously shown to form in the absence of metal with just carbon nanotubes and salt flux. This confirms the fact that small amounts of potassium fluoride are required in the salt flux to form the important intermediate species MF_3 , which then led to product formation.

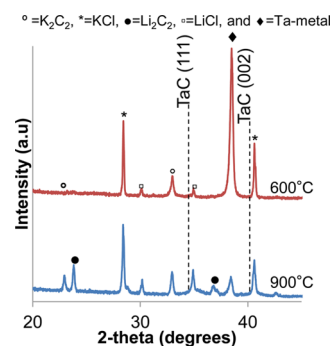


Figure 5. XRD plots of a control experiment for TaC using a KCl, LiCl salt flux without KF at 600 and 900 °C.

Additional control reactions were also run replacing the salt flux with a single fluoride (KF, LiF, and NaF) to further highlight the need for fluoride to form the carbide product and identify cation interaction. The experiments were conducted on TaC with the given salt at three temperature increments 300, 600, 900 °C and quenched. The XRD pattern of the 900 °C samples seen in Figure 6 show that TaC forms quickly and that

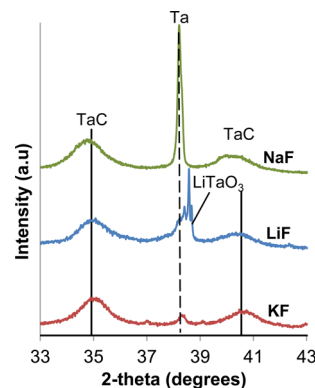


Figure 6. XRD plots of products from Ta and MWCNTs heated to 900 °C in pure KF, LiF, and NaF.

the reaction nearly goes to completion in the KF flux. From these results, it was determined that the best cation of the three single salts was potassium, based on the metal-to-carbide ratio in the final product seen in Figure 6. This supports our proposed mechanism with the formation of carbide via the intermediates MF_3 and K_2C_2 .

The final step of the proposed mechanism seen in eq 3 involves a solid-state metathesis reaction. These reactions are thermodynamically favored involving chemical exchange and the rapid often violent release of excess energy.³⁸ This has been shown to be an effective method for producing transition metal carbides, and in a previous report TaCl_5 and CaC_2 were mixed in stoichiometric amounts and underwent filament-initiated reaction to produce TaC.³⁸ For the purposes of this paper the metal fluoride, TaF_5 , and carbide, CaC_2 , were chosen to mimic the observed intermediates TaF_3 and K_2C_2 due to their commercial availability. They were combined stoichiometrically under argon, and the reaction was studied with DSC. The precursors were heated at 10 °C per minute to 400 and 800 °C. In Figure 7a, the experiment ran to 800 °C shows an endothermic event occurring at 383 °C before quickly becoming exothermic. According to the XRD plot shown in Figure 7b, TaC is present at 400 °C indicating that the

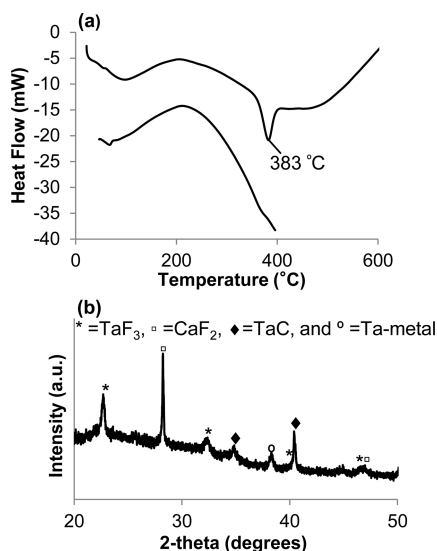


Figure 7. (a) DSC of TaF₅ and CaC₂ heated under argon to 400 and 800 °C with a ramp rate of 10 °C/min. (b) Resulting XRD plot of the 400 °C sample. Note: exothermic is up.

presence of intermediates (K₂C₂ and TaF₃) in the beginning of the reaction would further lower the temperature of product formation. This provides conclusive evidence supporting the formation mechanism. Note that the second peak for TaC is unusually intense due to excess TaF₃. To highlight the necessity of the halide intermediates, a similar experiment was conducted using Ta metal and CaC₂ as seen in Supporting Information, Figure S7. When heating only Ta metal and CaC₂ to 400 and 800 °C, no noticeable reaction occurs verified by the presence of reactants via XRD and the lack of the endothermic peak in the DSC trace. This further verifies the need for fluorine in these reactions and the crucial role that the fluoride intermediate species plays.

CONCLUSION

Salt flux synthesis reactions provide a low-temperature, and thus efficient, approach to synthesize transition metal carbides as nanomaterials. Understanding how the salt flux interacts with the metal and carbon to produce metal carbides offers an insight into the reaction mechanism and opens the door for optimization of the reaction. Because of the similarities of observed reaction intermediates (K₂C₂ and metal trifluorides), these reactions can easily be adapted to a wide variety of monometallic and more complicated bimetallic carbide systems. Further investigation will allow for difficult monometallic carbides to be synthesized more efficiently and also adapt the system to synthesize more complicated multimetallic carbides. In addition, determining what intermediates form at specific temperatures will enable researchers to establish temperatures of formation for various products and take the guesswork out of the synthesis process. Finally, using the salt flux as a trapping medium for intermediate species will also enable other types of products to be studied spectroscopically. Salt flux syntheses are well-known solid state reactions forming a variety of products (oxides, pnictides, chalcogenides, halides, and carbides), and since the fluxes are generally transparent to spectroscopic techniques, they can now be studied mechanistically.

ASSOCIATED CONTENT

Supporting Information

Table of XRD peak positions and associated reflections; additional experimental results analyzed by XRD; SEM and TEM of starting materials and products; XRD and DSC control experiments of TaC with and without KF; and Ta-metal and CaC₂. This material is available free of charge via the Internet at <http://pubs.acs.org>.

AUTHOR INFORMATION

Corresponding Author

*E-mail: bleonar5@uwyo.edu.

Notes

The authors declare no competing financial interest.

REFERENCES

- Oyama, S. T. *The Chemistry of Transition Metal Carbides and Nitrides*; Springer: Glasgow, 1996.
- Samsonov, G.; Vinitiskii, I. *Handbook of Refractory Compounds*; Plenum: New York, 1980.
- Goldschmidt, H. *Interstitial Alloys*; Plenum: New York, 1967.
- Toth, L. *Transition Metal Carbide and Nitrides, General Properties, Preparation and Characterization*; Academic Press: New York, 1971.
- Dash, T.; Nayak, B.; Abhangi, M.; Makwana, R.; Vala, S.; Jakhar, S.; Rao, C.; Basu, T. *Fusion Sci. Technol.* **2014**, *65*, 241–247.
- Racault, C.; Langlais, F.; Naslain, R. *J. Mater. Sci.* **1994**, *29*, 3384–3392.
- Niksirat, S.; Raygan, S. *Adv. Powder Technol.* **2014**, *25*, 859–864.
- Nelson, J.; Wagner, M. *Chem. Mater.* **2002**, *14*, 1639–1642.
- Johnson, C.; Sellinschegg, H.; Johnson, D. *Chem. Mater.* **2001**, *13*, 3876–3881.
- Suslick, K.; Hyeon, T.; Fang, M.; Cichowlas, A. *MRS Online Proc. Libr.* **1994**, 351.
- Suslick, K.; Reisse, J.; Mason, T.; Crum, L. *Sonochemistry and Sonoluminescence*; Springer: Netherlands, 1999.
- Li, X.; Westwood, A.; Brown, A.; Brydson, R.; Rand, B. *Carbon* **2009**, *47*, 201–208.
- Liu, X.; Fechler, N.; Antonietti, M. *Chem. Soc. Rev.* **2013**, *42*, 8237–8265.
- Chance, W.; zur Loye, H. *Solid State Sci.* **2014**, *28*, 90–94.
- Chan, J.; Kauzlarich, S. *Chem. Mater.* **1997**, *9*, 531–534.
- Kanatzidis, M.; Pöttgen, R.; Jeitschko, W. *Angew. Chem., Int. Ed.* **2005**, *44*, 6996–7023.
- Williamson, R.; Boo, W. *Inorg. Chem.* **1977**, *16*, 649–651.
- Foeppl, H. *Angew. Chem.* **1958**, *70*, 401.
- Zibrowius, B.; Bahtz, C.; Knapp, M.; Ruschewitz, U. *Phys. Chem. Chem. Phys.* **2004**, *6*, 5237–5243.
- Sandor, E.; Wooster, W. *Nature* **1958**, *182*, 1435–1436.
- Pessall, N.; Gold, R.; Johansen, H. *J. Phys. Chem. Solids* **1968**, *29*, 19–38.
- Hong, Y.; Williamson, R.; Boo, W. *Inorg. Chem.* **1979**, *18*, 2123–2125.
- Hong, Y.; Williamson, R.; Boo, W. *Inorg. Chem.* **1980**, *19*, 2229–2233.
- Hong, Y.; Williamson, R.; Boo, W. *Inorg. Chem.* **1981**, *20*, 403–409.
- Boo, W.; Williamson, R.; Baker, K.; Hong, Y. *Mol. Cryst. Liq. Cryst.* **1984**, *107*, 195–210.
- Yeh, Y.; Hong, Y.; Boo, W.; Mattern, D. *J. Solid State Chem.* **2005**, *178*, 2191–2196.
- Cros, C. *Rev. Chim. Miner.* **1974**, *11*, 585–591.
- Ruschewitz, U. *Coord. Chem. Rev.* **2003**, *244*, 115–136.
- Li, W.; Zhang, H.; Wang, C.; Zhang, Y.; Xu, L.; Zhu, K.; Xie, S. *Appl. Phys. Lett.* **1997**, *70*, 2684–2686.
- Tuinstra, F.; Koenig, J. *J. Chem. Phys.* **1970**, *53*, 1126–1130.
- Hiura, H.; Ebbesen, T.; Tanigaki, K.; Takahashi, H. *Chem. Phys. Lett.* **1993**, *202*, 509–512.

- (32) Pretsch, E.; Clerc, T.; Seibl, J. *Tables of Spectral Data for Structure Determination of Organic Compounds; [¹³C-NMR, ¹H-NMR, IR, MS, UV/VIS]*; Springer: Berlin, 1989.
- (33) Siegel, S. *Acta Crystallogr.* **1956**, *9*, 684.
- (34) Gutman, V.; Jack, K. *Acta Crystallogr.* **1951**, *4*, 244–246.
- (35) Elliott, R.; Kempter, C. *J. Phys. Chem.* **1958**, *62*, 630–631.
- (36) Fukunaga, A.; Chu, S.; McHenry, M. J. *Mater. Res.* **1998**, *13*, 2465–2471.
- (37) Becker, K.; Ebert, F. Z. *Phys.* **1925**, *31*, 268.
- (38) Nartowski, A.; Parkin, I.; MacKenzie, M.; Craven, A.; MacLeod, I. J. *Mater. Chem.* **1999**, *9*, 1275–1281.